

**Electronic Supplementary Information
A New Way of Studying Chemical Reactions: A Hand-in-Hand URVA and
QTAIM Approach**

Sadisha Nanayakkara and Elfi Kraka

Computational and Theoretical Chemistry Group (CATCO),
Department of Chemistry, Southern Methodist University,
3215 Daniel Avenue, Dallas, Texas 75275-0314, United States
ekraka@smu.edu
<http://www.smu.edu/catco>

Study of bond formation/cleavage mechanisms with combined URVA and QTAIM approach for R3, R5-R8 and R10.

3.1. R3: Isomerization of HN_2^+ This reaction proceeds via transfer of H from one N terminal to the other. The curvature of the proton transfer reaction in HN_2^+ has one peak appearing at the TS ($s = 0$ units). These contributions come from the cleaving bond N1H3 and the forming bond N2H3; both having supportive components to the curvature peak. This is the exact point where decisive changes in the ED topology take place. A bond catastrophe structure of the conflict type [1, 2] is found at this E point ($s = 0$ units) in which the N1H3 bond path disappears and the N2H3 bond path appears (see Figure S1-B). The overlapping curvature components of the forming/cleaving bonds at the curvature peak suggest these events are synchronized. This is confirmed by the ED analysis. The existence of a bond path only between N2H3 atomic basins but not for both (or in other words the absence of a ring critical point) at this E point, indicates the simultaneous breaking of the N1H3 bond and forming of the N2H3 bond in a concerted-type mechanism. Here, at N2H3, $H(c)$ is negative which is characteristic of its covalent nature. Another notable change in the topological features of N2H3 at curvature peak, is the high ellipticity ε (=0.77, see Table S7) which gradually falls off to zero at the very end of the reaction path corresponding to the product. As observed in previous studies [3–5], ellipticity could be used as a sensitive index for retrieving information about the anisotropy of the electron density upon bond formation. The large ε value at the curvature peak conforms with the T-shaped topology of the Laplacian, suggesting the formation of a classical π -complex (see Figure S1-B). Additionally, this reaction can be viewed as a special case where TS serves as a center for bond cleavage and formation as it is coupled with the curvature peak. Furthermore, beginning from M1 up to the formation of a π -complex at TS, no intermediary 3-membered ring was

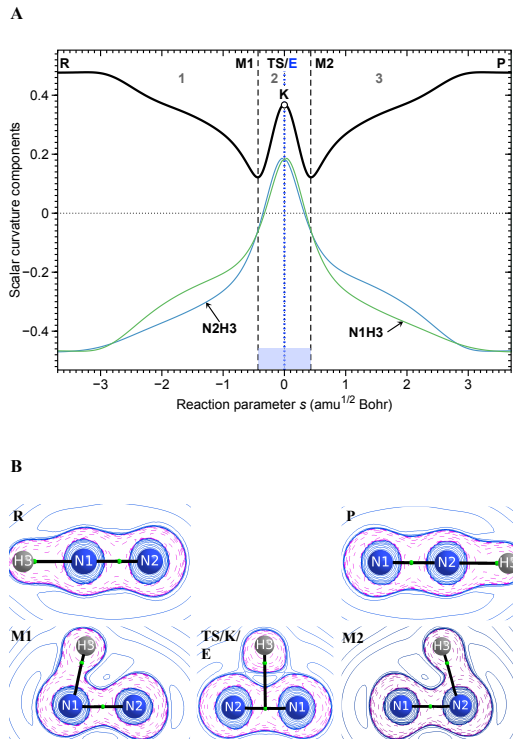


Fig. S1: R3 A) Scalar curvature as a function of the reaction parameter s (solid black line). The decomposition of scalar curvature into components is given in color. The borders of the reaction phases are indicated by vertical dashed lines at curvature points M1, M2, M3, etc. The TS at $s = 0 \text{ amu}^{1/2} \text{ Bohr}$ is also indicated by a vertical dashed line. R and P mark the first and last curvature points, corresponding to reactant and product respectively. K denotes a curvature peak. E denotes a special point in electron density shown by a blue vertical dashed line. Values in grey 1, 2, 3, etc. indicate reaction phases and highlighted region in blue shows the chemical phases. B) Laplacian contour plots of selected curvature points R, M1, TS/K/E, M2, and P, plotted in the molecular plane. The dashed (pink) contours denote regions of charge concentration where $\nabla^2\rho(\mathbf{r}) < 0$, and the solid (blue) contours denote regions of charge depletion where $\nabla^2\rho(\mathbf{r}) > 0$.

Table S1: Local topological properties of the electron density $\rho(c)$ calculated at the bond critical points c along the IRC for the forming bond N2H3 and cleaving bond N1H3; values in bold are for curvature peak data. s reaction parameter, $\rho(c)$ electron density, $\nabla^2 \rho(c)$ Laplacian, $H(c)$ total energy density, ε ellipticity calculated at the MP2/6-31G(d,p) level of theory

Numbering	Bond	Character	s (amu $^{1/2}$ Bohr)	$\rho(c)$ (e/Bohr 3)	$\nabla^2 \rho(c)$ (e/Bohr 5)	ε	$H(c)$ (Hartree/Bohr 3)
$\text{H}_3-\overset{\oplus}{\text{N}}=\text{N}_2 \longrightarrow \text{N}=\overset{\oplus}{\text{N}}_2-\text{H}_3$	N1H3	R	-3.7909	0.2907	-1.7438	0.0000	-0.4624
		M1	-0.4399	0.2141	-0.6668	0.2169	-0.2401
		TS/K/E	0.0000	-	-	-	-
		M2	0.4399	-	-	-	-
		P	3.7909	-	-	-	-
	N2H3	R	-3.7909	-	-	-	-
		M1	-0.4399	-	-	-	-
		TS/K/E	0.0000	0.1817	-0.5079	0.7741	-0.1955
		M2	0.4399	0.2141	-0.6668	0.2169	-0.2401
		P	3.7909	0.2907	-1.7438	0.0000	-0.4624

observed which is a common misconception involved in the event of π -complex generation. Since, a bond catastrophe E point and a curvature peak coincide on the reaction path, this reaction is a compelling case showing how features in the PES are smoothly transferred over to the ED.

3.2. R5: β -hydride elimination of ethylgold (III) dichloride β -hydride elimination reactions of gold(III) complexes are commonplace reactions in organometallic chemistry [6, 7] and studied in a number of synthetic/computational works [8, 9]. Recent URVA studies have elaborated on its reaction mechanism as means of gaining solid understanding for the rational design of gold catalysts for β -hydride elimination [10]. Here, we emphasize on the topological changes of electron density leading to the coordination of H to Au, with the aim of locating and describing the interesting intermediate points along the IRC. According to URVA curvature, most of the reaction path is dedicated to the preparation of the RC (i.e. conformational changes) prior to actual bond formation/cleavage processes which take place within a short chemical phase. At K5 curvature peak in phase 8, the dominant supporting contribution comes from the C4H10 bond cleavage component accompanied by the Au2C4 and Au2H10 bond formation components. A bond path corresponding to the latter first appears at E1($=-3.87$ s) signifying the formation of an agostic Au-H interaction. Here, E1 (see Figure S2-B) is a significant catastrophe point, known as a catastrophe point of bifurcation type [1, 2] where a merged bond and ring critical point is found associated with the Au2H10 bond path and H10-Au2-C1-C4 ring. This coalescence of bond and ring critical points is reflected in very large ε values ($=14.9$, see Table S2) at Au2H10, typical of catastrophe structures [11]. Additionally, it is seen from the curvature that Au2H10 component becomes resisting after E1. It is worth mentioning that, although the nonclassical 2e-3c Au2C4 bond formation has been revealed by curvature peak K5, a bond path between Au2C4 could not be detected as was observed in few instances involving metal and terminal C interactions [12, 13]. At the beginning of the entrance channel, ethyl ligand is in a σ type of interaction with the Au center which in turn converts to a π type of interaction towards the exit channel. This is reflected in ε values for Au2C1 which increases from R to P, signifying the generation of a π -complex between gold (III) and ethylene. Shortly after the TS ($+0.27$ s units at E2, see Figure S2-B), the C4H10 bond path disappears giving rise to another bifurcation point. Here, we point out that when locating E2 associated with C4H10 cleavage, priority was given to locating the bifurcation point over ceasing of VSAC overlap between C4 and H10 atomic basins, besides Laplacian being the better probe in general. But it can be understood from the ED distributions at K5 and TS (see Figure S2-B) that VSAC overlap point will also be located in-between this path region after K5 peak similar to the bifurcation point. In connection to curvature, C4H10 is already resisting at E2 and Au2H10 turns into a slightly supporting contribution. Overall, E1 associated with the Au2H10 bond formation occurred before its respective curvature peak and E2 linked to the C4H10 bond cleavage followed after the curvature peak.

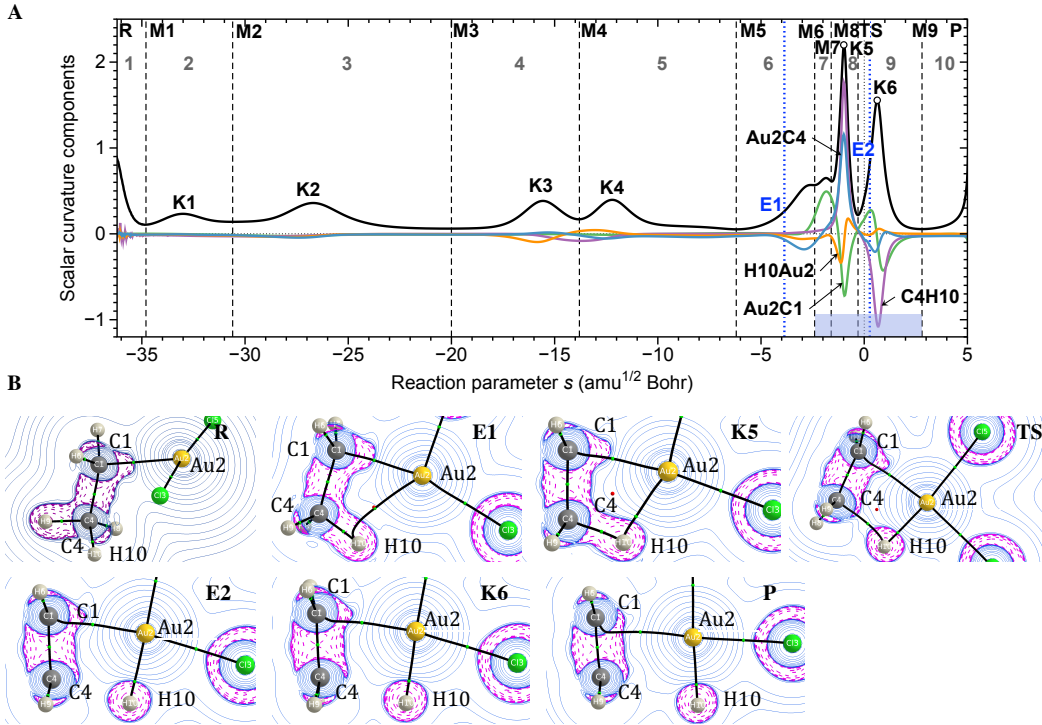


Fig. S2: R5 A) Scalar curvature as a function of the reaction parameter s (solid black line). The decomposition of scalar curvature into components is given in color. The borders of the reaction phases are indicated by vertical dashed lines at curvature points M1, M2, M3, etc. The TS at $s = 0 \text{ amu}^{1/2}$ Bohr is also indicated by a vertical dashed line. R and P mark the first and last curvature points, corresponding to reactant and product respectively. K1, K2, etc. denote curvature peaks. E1, E2, etc. denote special points in electron density shown by blue vertical dashed lines. Values in grey 1, 2, 3, etc. indicate reaction phases and highlighted region in blue shows the chemical phases. B) Laplacian contour plots at selected curvature points R, E1, K5, TS, E2, K6, and P, plotted in the C1-C4-Au2 plane. The dashed (pink) contours denote regions of charge concentration where $\nabla^2 \rho(\mathbf{r}) < 0$, and the solid (blue) contours denote regions of charge depletion where $\nabla^2 \rho(\mathbf{r}) > 0$.

Table S2: Local topological properties of the electron density $\rho(c)$ along the IRC calculated at the bond critical points c for the selected bonds Au2H10,C4H10,Au2C1; values in bold are for curvature peak data. s reaction parameter, $\rho(c)$ electron density, $\nabla^2\rho(c)$ Laplacian, $H(c)$ total energy density, ε ellipticity calculated at the B3LYP/Def2-SVP/Au(ECP) level of theory

Numbering	Bond	Character	s (amu $^{1/2}$ Bohr)	$\rho(c)$ (e/Bohr 3)	$\nabla^2\rho(c)$ (e/Bohr 5)	ε	$H(c)$ (Hartree/Bohr 3)
	Au2C1	R	-36.2625	0.1119	-0.0038	0.0034	-0.0527
		M1	-34.8528	0.1118	-0.0036	0.0069	-0.0527
		M2	-30.6236	0.1108	-0.0020	0.0232	-0.0517
		M3	-20.2157	0.1111	0.0001	0.0352	-0.0516
		M4	-13.8270	0.1156	0.0011	0.0404	-0.0549
		M5	-6.2086	0.1253	0.0133	0.0333	-0.0625
		E1	-3.8691	0.1254	0.0277	0.0220	-0.0624
		M6	-2.4294	0.1236	0.0421	0.0010	-0.0609
		M7	-1.5595	0.1149	0.0604	0.0443	-0.0531
		K5	-0.9897	0.1042	0.0796	0.1196	-0.0439
		M8	-0.2999	0.0956	0.1098	0.2878	-0.0363
		TS	0.0000	0.0924	0.1213	0.3843	-0.0335
		E2	0.2699	0.0895	0.1295	0.4784	-0.0310
		K6	0.6298	0.0855	0.1368	0.6197	-0.0276
		M9	2.8193	0.0771	0.1480	1.2003	-0.0203
		P	5.1053	0.0731	0.1599	2.4666	-0.0158
	Au2H10	R	-36.2625	-	-	-	-
		M1	-34.8528	-	-	-	-
		M2	-30.6236	-	-	-	-
		M3	-20.2157	-	-	-	-
		M4	-13.8270	-	-	-	-
		M5	-6.2086	-	-	-	-
		E1	-3.8691	0.0441	0.1683	14.8562	-0.0023
		M6	-2.4294	0.0606	0.1745	0.6970	-0.0112
		M7	-1.5595	0.0789	0.1952	0.4593	-0.0213
		K5	-0.9897	0.0979	0.1931	0.2915	-0.0354
		M8	-0.2999	0.1315	0.0848	0.0764	-0.0716
		TS	0.0000	0.1435	0.0346	0.0397	-0.0862
		E2	0.2699	0.1516	-0.0033	0.0192	-0.0965
		K6	0.6298	0.1584	-0.0390	0.0023	-0.1055
		M9	2.8193	0.1646	-0.0726	0.0151	-0.1134
		P	5.1053	0.1662	-0.0788	0.0196	-0.1148
	C4H10	R	-36.2625	0.2735	-1.0146	0.0076	-0.2917
		M1	-34.8528	0.2741	-1.0220	0.0072	-0.2931
		M2	-30.6236	0.2761	-1.0435	0.0062	-0.2974
		M3	-20.2157	0.2732	-1.0085	0.0071	-0.2907
		M4	-13.8270	0.2675	-0.9620	0.0119	-0.2809
		M5	-6.2086	0.2499	-0.8143	0.0117	-0.2486
		E1	-3.8691	0.2352	-0.6980	0.0084	-0.2221
		M6	-2.4294	0.2192	-0.5792	0.0042	-0.1942
		M7	-1.5595	0.2021	-0.4635	0.0021	-0.1660
		K5	-0.9897	0.1754	-0.3118	0.0139	-0.1261
		M8	-0.2999	0.0961	-0.0323	0.1796	-0.0406
		TS	0.0000	0.0738	0.0249	0.5374	-0.0227
		E2	0.2699	-	-	-	-
		K6	0.6298	-	-	-	-
		M9	2.8193	-	-	-	-
		P	5.1053	-	-	-	-

3.3. R6: Diels-Alder reaction between Ethene and gauche 1,3-butadiene This reaction has been extensively studied under symmetry-allowed pericyclic reactions in many viewpoints [14, 15]. Nonetheless, there is only a handful of occasions [16, 17], including the preceding URVA studies [18, 19], where it was particularly focused on following the reaction path to identify and analyze exact positions of CC σ bond formations, hence our goal to pursue in this combined study. In the curvature profile, there is one major peak K1 at +5 s units appearing towards the very end of the exit channel (see Figure S3-A) which is caused by the formation of equivalent bonds C2C8 and C1C7. Topological analysis at K1 (see Figure S3-B) shows accumulation of charge density between both C1C7 and C1C8 atomic basins, having negative $\nabla^2\rho(c)$ and $H(c)$ values (see Table S3) at the s. The initial VSCC overlap occurs at E1, which is very shortly after TS (+1 s units, see Figure S3-B) and located next to a curvature minima M4. Here, negative $\nabla^2\rho(c)$ and $H(c)$ values are evidence of the formation of the new CC σ bond pair. It has been revealed by URVA analysis that prior to CC bond formation, pyramidalization at the terminal C atoms takes place (i.e. C1, C2, C7, C8; at the four reacting centers) and in this sense M4 has been recognized as a mechanistically important curvature point. The inflection point for the pyramidalization curves for four terminal C atoms occurs at M4 and it is interesting to see decisive changes in the ED also happening onwards this point. Also, it can be seen from curvature that C1C2 component becomes resisting after E1 which is connected with rehybridization of those C atoms as a direct consequence of pyramidalization. It is clear that the E1 point associated with CC σ bond formation precedes the curvature peak and a more significant revelation is that it occurs rather close to a curvature minima identified as a mechanistically important reference point.

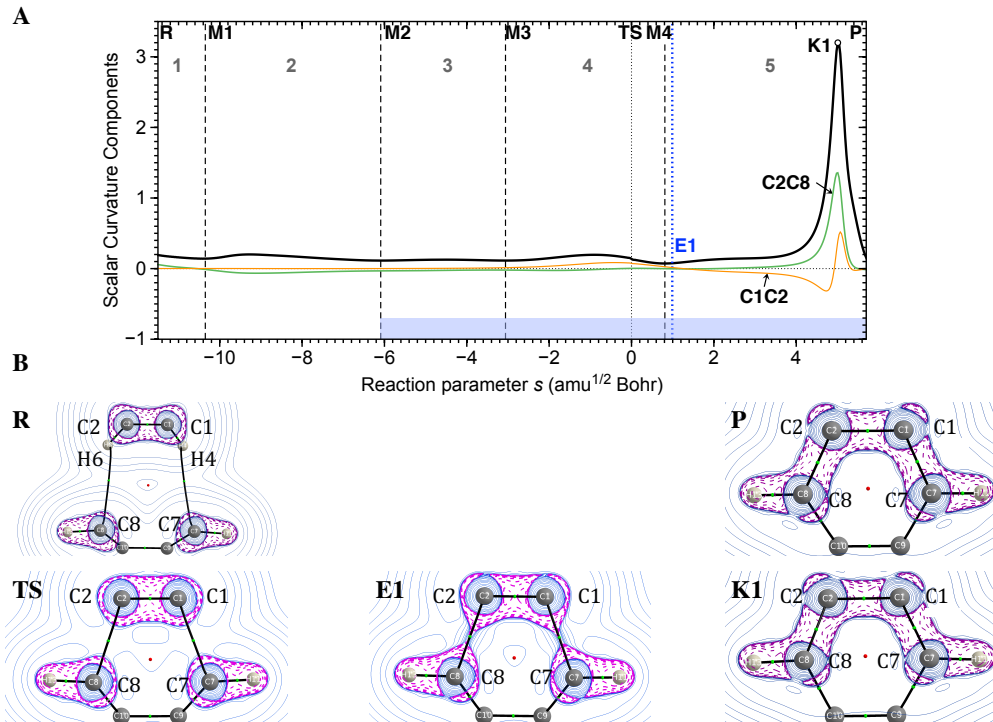


Fig. S3: **R6** A) Scalar curvature as a function of the reaction parameter s (solid black line). The decomposition of scalar curvature into components is given in color. The borders of the reaction phases are indicated by vertical dashed lines at curvature points M1, M2, M3, etc. The TS at $s = 0$ amu^{1/2} Bohr is also indicated by a vertical dashed line. R and P mark the first and last curvature points, corresponding to reactant and product respectively. K1, K2, etc. denote curvature peaks. E1, E2, etc. denote special points in electron density shown by blue vertical dashed lines. Values in grey 1, 2, 3, etc. indicate reaction phases and highlighted region in blue shows the chemical phases. B) Laplacian contour plots of selected curvature points R, TS, E1, K1, and P, plotted in the C1-C2-C8 plane. Some H atoms omitted for clarity. The dashed (pink) contours denote regions of charge concentration where $\nabla^2\rho(\mathbf{r}) < 0$, and the solid (blue) contours denote regions of charge depletion where $\nabla^2\rho(\mathbf{r}) > 0$.

Table S3: Local topological properties of the electron density $\rho(c)$ along the IRC calculated at the bond critical points c for the forming bonds C2C8/C1C7; values in bold are for curvature peak data. s reaction parameter, $\rho(c)$ electron density, $\nabla^2\rho(c)$ Laplacian, $H(c)$ total energy density, ε ellipticity calculated at the B3LYP/6-31G(d,p) level of theory

Numbering	Bond	Character	s (amu $^{1/2}$ Bohr)	$\rho(c)$ (e/Bohr 3)	$\nabla^2\rho(c)$ (e/Bohr 5)	ε	$H(c)$ (Hartree/Bohr 3)
		C2C8/C1C7					
		R	-11.5195	-	-	-	-
		M1	-10.3495	0.0045	0.0130	1.5565	0.0007
		M2	-6.0895	0.0091	0.0255	0.4483	0.0011
		M3	-3.0595	0.0187	0.0517	0.3656	0.0014
		TS	0.0000	0.0508	0.0463	0.0970	-0.0089
		M4	0.8096	0.0701	0.0087	0.0585	-0.0192
		E1	0.9896	0.0747	-0.0018	0.0529	-0.0220
		K1	5.0094	0.2333	-0.5051	0.0087	-0.1796
		P	5.7893	0.2361	-0.5178	0.0088	-0.1834

3.4. R7: Ring-closure of 1,2,4,6-Heptatetraene This reaction often used as a reference for differentiating between pericyclic and *psuedopericyclic* reactions [20] has been investigated in detail, using topological features of electron density [4] as well as by molecular orbitals analysis [21, 22] and further insight was provided with URVA studies [23]. According to the curvature profile, the reaction proceeds via the formation of C1C6 σ bond resulting in the K1 peak at +4.50 s units (see Figure S4-A). The charge densities concentrated around C1 and C6 atomic basins come in

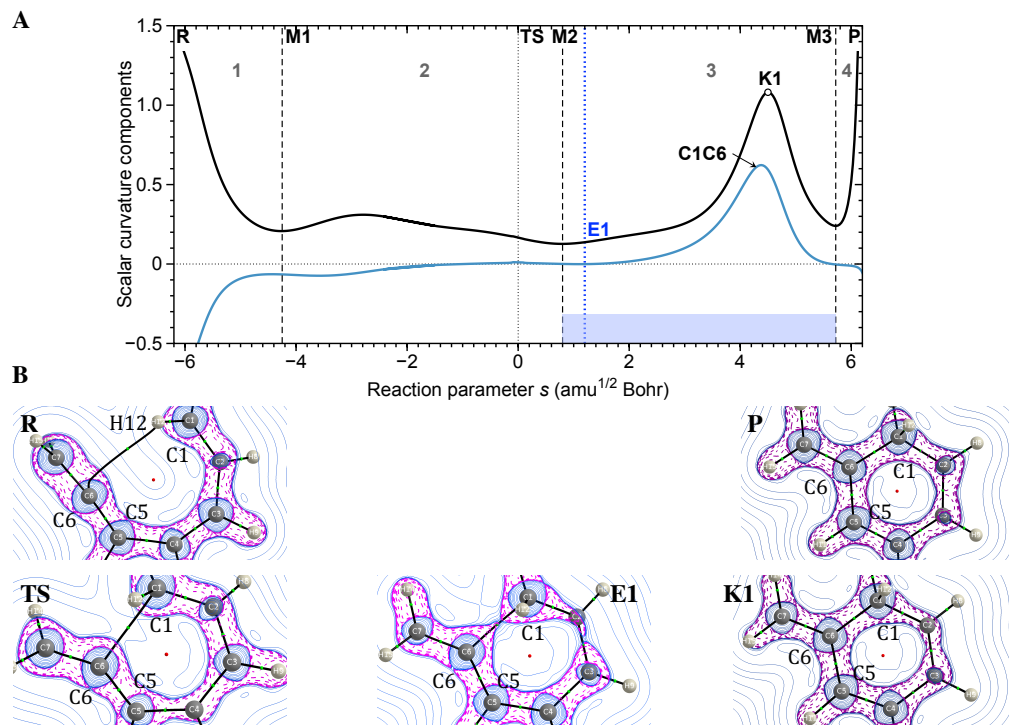
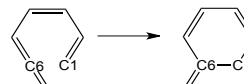


Fig. S4: **R7** A) Scalar curvature as a function of the reaction parameter s (solid black line). The decomposition of scalar curvature into components is given in color. The borders of the reaction phases are indicated by vertical dashed lines at curvature points M1, M2, M3, etc. The TS at $s = 0$ amu $^{1/2}$ Bohr is also indicated by a vertical dashed line. R and P mark the first and last curvature points, corresponding to reactant and product respectively. K1, K2, etc. denote curvature peaks. E1, E2, etc. denote special points in electron density shown by blue vertical dashed lines. Values in grey 1, 2, 3, etc. indicate reaction phases and highlighted region in blue shows the chemical phases. B) Laplacian contour plots of selected curvature points R, TS, E1, K1, and P, plotted in the C1-C6-C5 plane. The dashed (pink) contours denote regions of charge concentration where $\nabla^2\rho(\mathbf{r}) < 0$, and the solid (blue) contours denote regions of charge depletion where $\nabla^2\rho(\mathbf{r}) > 0$.

Table S4: Local topological properties of the electron density $\rho(c)$ along the IRC calculated at the bond critical points c for the forming bond C1C6; values in bold are for curvature peak data. s reaction parameter, $\rho(c)$ electron density, $\nabla^2\rho(c)$ Laplacian, $H(c)$ total energy density, ε ellipticity calculated at the B3LYP/6-311+G(d,p) level of theory

Numbering	Bond	Character	s (amu $^{1/2}$ Bohr)	$\rho(c)$ (e/Bohr 3)	$\nabla^2\rho(c)$ (e/Bohr 5)	ε	$H(c)$ (Hartree/Bohr 3)
	C1C6	R	-6.2387	-	-	-	-
		M1	-4.2591	-	-	-	-
		TS	0.0000	0.0487	0.0535	0.3111	-0.0077
		M2	0.8098	0.0700	0.0181	0.1774	-0.0177
		E1	1.1997	0.0829	-0.0076	0.1401	-0.0249
		K1	4.4990	0.2374	-0.5262	0.0422	-0.1852
		M3	5.7288	0.2449	-0.5651	0.0365	-0.1967
		P	6.2684	0.2449	-0.5656	0.0353	-0.1967

contact at E1 (initial VSCC overlap), +1.2 s units after TS as shown by its respective Laplacian topology (see Figure S4-B), developing a covalent interaction as confirmed by the slightly negative $H(c)$ (see Table S4). Afterwards, $H(c)$ progressively increases establishing the C1C6 bond at K1, also clear by the dense charge build-up between C1C6 as indicated by K1 contour plot (see Figure S4-B). Here, it is interesting to see in comparison to the Diels-Alder reaction **R5**, not only the curvature shapes indicating the formation of the CC σ bond/s are similar but also the relative locations of the E points associated with it. In addition, both of these reactions are typical examples demonstrating that TS is not so an important center for the bond formation/cleavage processes as confirmed by the curvature and the ED analysis too. We can see a nice continuum to the previously identified connection between PES and ED where E1 point associated with the CC bond formation event occurred before and close to the curvature peak.

3.5. R8: 1,3-dipole cycloaddition of HCNO to acetylene 1,3-dipole cycloaddition reactions are vastly studied using several quantum chemical tools [24–27] involving the URVA analysis [28, 29] to answer many underlying mechanistic questions regarding its reaction mechanism. In line with the previous work [28, 29], we focus on this particular reaction as a good candidate to study the asynchronicity of bond formation when 1,3-dipoles of HCNO react with acetylene dipolarophile to generate a five-membered ring containing N and O heteroatoms. The first VSCC overlap (E1, see Figure S5-B) of the C2C3 bond formation takes place before K3 peak, just after +1.26 s units from TS, also reflected by the sign change of $\nabla^2\rho(c)$ from positive to negative, and negative $H(c)$ values (see Table S5) indicating the covalent nature. Since then $H(c)$ progressively increases establishing covalent character of C2C3 at peak K3. At this peak, opposed to the supporting contribution from C2C3, C1O4 is still showing a resistance to bond formation. This is also clearly visible in the Laplacian topology of the RC at K3 peak. There is no accumulation of charge density between C1O4 atomic basins at peak K3 as shown by positive $\nabla^2\rho(c)$ (=0.08, see Table S5), confirming that the more polar C1O4 bond will be formed later. In fact, this asynchronicity in the bond formation was quantified in the URVA analysis, which was reported to be the highest for this particular reaction [29]. The VSCC overlap starts to develop between the C1O4 atomic basins at +5.80 s units (E2, see Figure S5-B) which gradually increases towards P favoring the formation of C1O4. The relative locations of the E and K points are consistent with former observations where changes in the ED preceded that of PES in the process of a new bond formation, in this case C2C3 and C1O4 bonds.

Table S5: Local topological properties of the electron density $\rho(c)$ along the IRC calculated at the bond critical points c for the forming bonds C2C3 and C1O4; values in bold are for curvature peak data. s reaction parameter, $\rho(c)$ electron density, $\nabla^2\rho(c)$ Laplacian, $H(c)$ total energy density, ε ellipticity calculated at the B3LYP/6-31G(d,p) level of theory

Numbering	Bond	Character	s (amu $^{1/2}$ Bohr)	$\rho(c)$ (e/Bohr 3)	$\nabla^2\rho(c)$ (e/Bohr 5)	ε	$H(c)$ (Hartree/Bohr 3)
$\text{H}_8-\text{C}1\equiv\text{C}3-\text{H} + \text{H}-\text{C}2=\text{N}-\text{O} \longrightarrow$	C2C3	R	-10.8397	-	-	-	-
		M1	-4.4597	-	-	-	-
		TS	0.0000	0.0527	0.0663	0.0477	-0.0088
		M2	0.1997	0.0581	0.0594	0.0602	-0.0115
		E1	1.2597	0.0893	-0.0015	0.1000	-0.0308
		K3	4.1397	0.2325	-0.4711	0.1511	-0.1796
		E2	5.7997	0.2778	-0.6763	0.1650	-0.2500
		M3	6.2197	0.2829	-0.6994	0.1695	-0.2588
		P	7.2371	0.2941	-0.7490	0.1871	-0.2800
	C1O4	R	-10.8397	-	-	-	-
		M1	-4.4597	0.0119	0.0399	0.4889	0.0011
		TS	0.0000	0.0306	0.0775	0.0019	0.0004
		M2	0.1997	0.0324	0.0785	0.0142	0.0002
		E1	1.2597	0.0417	0.0813	0.0720	-0.0013
		K3	4.1397	0.0898	0.0808	0.1511	-0.0194
		E2	5.7997	0.1745	-0.1307	0.1515	-0.1158
		M3	6.2197	0.2069	-0.3058	0.1466	-0.1885
		P	7.2371	0.2990	-0.1118	0.0852	-0.4663

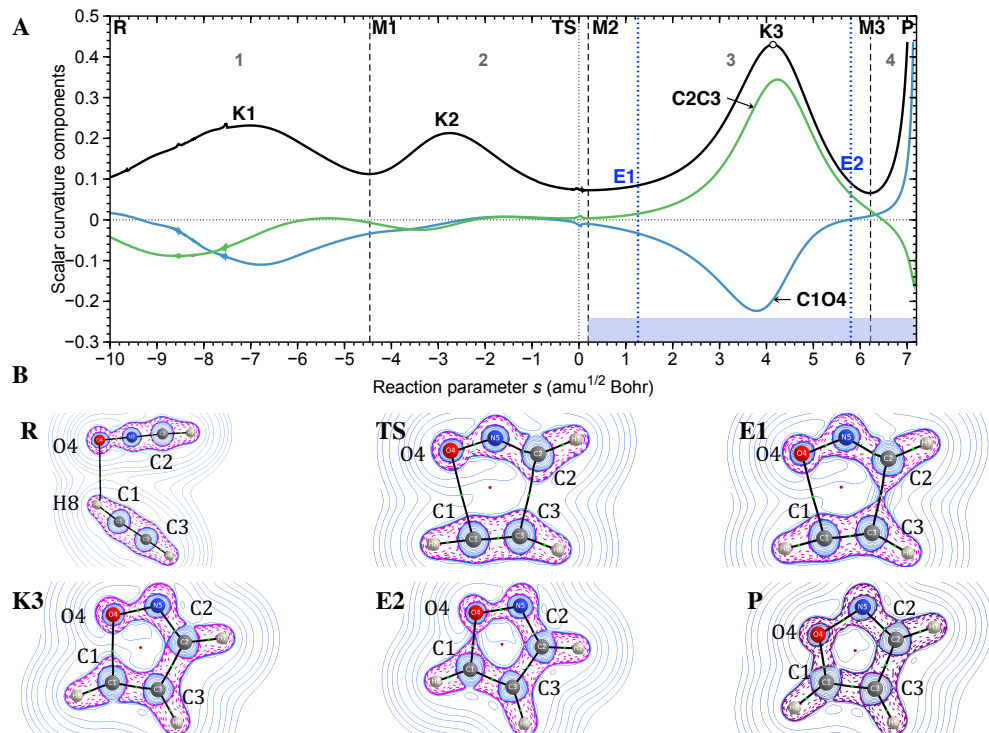


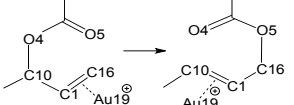
Fig. S5: **R8** A) Scalar curvature as a function of the reaction parameter s (solid black line). The decomposition of scalar curvature into components is given in color. The borders of the reaction phases are indicated by vertical dashed lines at curvature points M1, M2, M3, etc. The TS at $s = 0$ amu $^{1/2}$ Bohr is also indicated by a vertical dashed line. R and P mark the first and last curvature points, corresponding to reactant and product respectively. K1, K2, etc. denote curvature peaks. E1, E2, etc. denote special points in electron density shown by blue vertical dashed lines. Values in grey 1, 2, 3, etc. indicate reaction phases and highlighted region in blue shows the chemical phases. B) Laplacian contour plots of selected curvature points R, TS, E1, K3, E2, and P, plotted in the molecular plane (out of plane H are omitted). The dashed (pink) contours denote regions of charge concentration where $\nabla^2\rho(r) < 0$, and the solid (blue) contours denote regions of charge depletion where $\nabla^2\rho(r) > 0$.

3.6. R10: Gold(I)-catalyzed [3,3]-sigmatropic rearrangement of allyl acetate In this Au(I)-NHC-catalyzed 2-step reaction, Au-allyl acetate initially starts as a π -bonded complex and goes through an intermediate σ -bonded complex towards the end of the exit channel of step 1. It then reconfigures back into a π -bonded complex in step 2 [30]. URVA analysis of this reaction reveals four distinct curvature peaks (see Figure S6-B) for step 1. Most chemically significant events take place at peak K2 and K3, K2 being associated with loosening of the Au19C16 interaction whereas K3 corresponds to formation of the new C16O5 bond. Topological analysis shows a weak covalent interaction between Au and terminal C from the beginning of the reaction path as reflected by negative $H(c)$ values ($=-0.020$) at Au19C16 (see R in Table S6). Meanwhile, the bond between Au and central C, Au19C1, takes place much later at -5.05 s units (at E1, see Figure S6-B) before TS, resulting in a 3-membered ring between Au19-C1-C16 giving rise to a bifurcation type catastrophe point. Here, at E1, Au19C1 has a significant ε value ($=1.8$) resembling its π -character which rapidly approaches zero towards M7, signifying the transition of Au19C1 from a π bond to a σ bond. The loosening of Au19C16 interaction occurs at -4.30 s units (at E2, see Figure S6-B) before K2 peak located at -4.06 s units, which deviates from the trend observed so far where changes in the ED associated with a bond cleavage always followed after a peak. But this result is not surprising because as mentioned in connection with **R5** (see section 3.2.), detecting metal and terminal C interactions can often be elusive if one were to depend solely on presence/absence of bond paths [12, 13]. We continued to gather the ED at Au19C16 after its disappearance at few path points past K2 peak, and the decreasing negative $H(c)$ values suggest that the ED changes associated with bond cleavage are more likely to occur after the K2 peak as is consistent with former observations. New C16O5 starts to form at $+2.50$ s units (at E3, see Figure S6-B) as is reflected by negative $\nabla^2\rho(c)$ and $H(c)$ values (see Table S6) and at curvature peak K3 located at $+2.59$ s units, the bond formation is finalized (see Figure S6-B). The ε values for the C1C16 bond start fairly high and fall off to low values from R to M7, suggesting the conversion of the double bond between CC to a single bond by loosing its π character. In step 2 (see Figure S7), the Au19C1 interaction is established and the C1O4 bond is cleaved at peak K2 (see Figure S7-B) where the charge density ceases to flow between C10 and O4 atomic basins. Here, the significant changes in the ED displayed by E1, E2 and E3 and the subsequent curvature peaks are located in close proximity and in step 2, the E point coincides with K2 curvature peak.

Table S6: Local topological properties of the electron density $\rho(c)$ along the IRC calculated at the bond critical points c for the selected bonds Au19C16, Au19C1, C16O5, C1C16, O4C10; values in bold are for curvature peak data. s reaction parameter, $\rho(c)$ electron density, $\nabla^2\rho(c)$ Laplacian, $H(c)$ total energy density, ε ellipticity calculated at the B3LYP/6-31+G(d,p)/SDD level of theory

Numbering	Bond	Character	s (amu $^{1/2}$ Bohr)	$\rho(c)$ (e/Bohr 3)	$\nabla^2\rho(c)$ (e/Bohr 5)	ε	$H(c)$ (Hartree/Bohr 3)
Step1							
	Au19C16	R	-22.2851	0.0765	0.1593	1.0987	-0.0197
		M1	-20.7023	0.0764	0.1593	1.1060	-0.0197
		M2	-14.7935	0.0762	0.1574	1.0418	-0.0197
		K1	-10.8043	0.0761	0.1574	1.0492	-0.0195
		M3	-6.5751	0.0791	0.1643	1.2686	-0.0209
		E1	-5.0454	0.0801	0.1759	1.9602	-0.0205
		E2	-4.2956	-	-	-	-
		K2	-4.0557	-	-	-	-
		TS	0.0000	-	-	-	-
		M4	0.8461	-	-	-	-
		E3	2.4958	-	-	-	-
		K3	2.5858	-	-	-	-
		M5	3.1556	-	-	-	-
		M6	3.6954	-	-	-	-
		K4	4.3252	-	-	-	-
		M7	4.9250	-	-	-	-
Step2							
	Au19C1	R	-22.2851	-	-	-	-
		M1	-20.7023	-	-	-	-
		M2	-14.7935	-	-	-	-
		K1	-10.8043	-	-	-	-
		M3	-6.5751	-	-	-	-
		E1	-5.0454	0.0784	0.2047	1.8400	-0.0168
		E2	-4.2956	0.0804	0.1764	1.8319	-0.0208
		K2	-4.0557	0.0812	0.1695	1.3259	-0.0219
		TS	0.0000	0.0995	0.1492	0.0242	-0.0379
		M4	0.8461	0.1036	0.1579	0.0096	-0.0403
		E3	2.4958	0.1086	0.1695	0.0034	-0.0428
		K3	2.5858	0.1088	0.1698	0.0033	-0.0429

Continuation of Table S6

Numbering	Bond	Character	<i>s</i> (amu ^{1/2} Bohr)	$\rho(c)$ (e/Bohr ³)	$\nabla^2\rho(c)$ (e/Bohr ⁵)	ε	$H(c)$ (Hartree/Bohr ³)
	C16O5	M5 M6 K4 M7	3.1556 3.6954 4.3252 4.9250	0.1104 0.1117 0.1121 0.1120	0.1718 0.1733 0.1738 0.1736	0.0026 0.0022 0.0023 0.0023	-0.0440 -0.0451 -0.0454 -0.0453
		R M1 M2 K1 M3 E1 E2 K2 TS M4 E3 K3 M5 M6 K4 M7	-22.2851 -20.7023 -14.7935 -10.8043 -6.5751 -5.0454 -4.2956 -4.0557 0.0000 0.8461 2.4958 2.5858 3.1556 3.6954 4.3252 4.9250	- - - 0.0097 0.0146 0.0172 0.0190 0.0198 0.0665 0.0924 0.1678 0.1708 0.1803 0.1831 0.1843 0.1845	- - - 0.0367 0.0547 0.0643 0.0708 0.0735 0.1439 0.1263 -0.1362 -0.1500 -0.1890 -0.1990 -0.2031 -0.2039	- - - 2.4963 1.4636 0.9778 0.7379 0.6609 0.0937 0.0543 0.0259 0.0255 0.0220 0.0190 0.0175 0.0177	- - - 0.0015 0.0018 0.0019 0.0020 0.0020 -0.0093 -0.0260 -0.1467 -0.1548 -0.1819 -0.1901 -0.1934 -0.1940
	C1C16	R M1 M2 K1 M3 E1 E2 K2 TS M4 E3 K3 M5 M6 K4 M7	-22.2851 -20.7023 -14.7935 -10.8043 -6.5751 -5.0454 -4.2956 -4.0557 0.0000 0.8461 2.4958 2.5858 3.1556 3.6954 4.3252 4.9250	0.3246 0.3247 0.3251 0.3256 0.3264 0.3266 0.3268 0.3270 0.3059 0.2925 0.2653 0.2646 0.2631 0.2632 0.2631 0.2630	-0.9144 -0.9149 -0.9179 -0.9212 -0.9270 -0.9284 -0.9309 -0.9323 -0.8515 -0.7867 -0.6544 -0.6509 -0.6442 -0.6448 -0.6445 -0.6440	0.2355 0.2353 0.2341 0.2324 0.2262 0.2225 0.2195 0.2182 0.1478 0.1174 0.0566 0.0547 0.0482 0.0459 0.0449 0.0449	-0.3411 -0.3413 -0.3421 -0.3429 -0.3440 -0.3441 -0.3446 -0.3450 -0.3118 -0.2869 -0.2359 -0.2345 -0.2314 -0.2314 -0.2312 -0.2310
	O4C10	M1 M2 K2 M3 TS M4 M5 M6 P	-3.8155 -2.8559 -2.6160 -0.5765 0.0000 2.9225 6.6418 16.4198 21.8232	0.1669 0.1658 0.1641 0.0916 0.0735 0.0309 0.0158 - -	-0.1296 -0.1246 -0.1169 0.1261 0.1415 0.1004 0.0569 - -	0.0164 0.0169 0.0180 0.0607 0.0823 0.2211 0.9339 - -	-0.1469 -0.1442 -0.1400 -0.0260 -0.0134 0.0008 0.0017 - -
		Step 2					

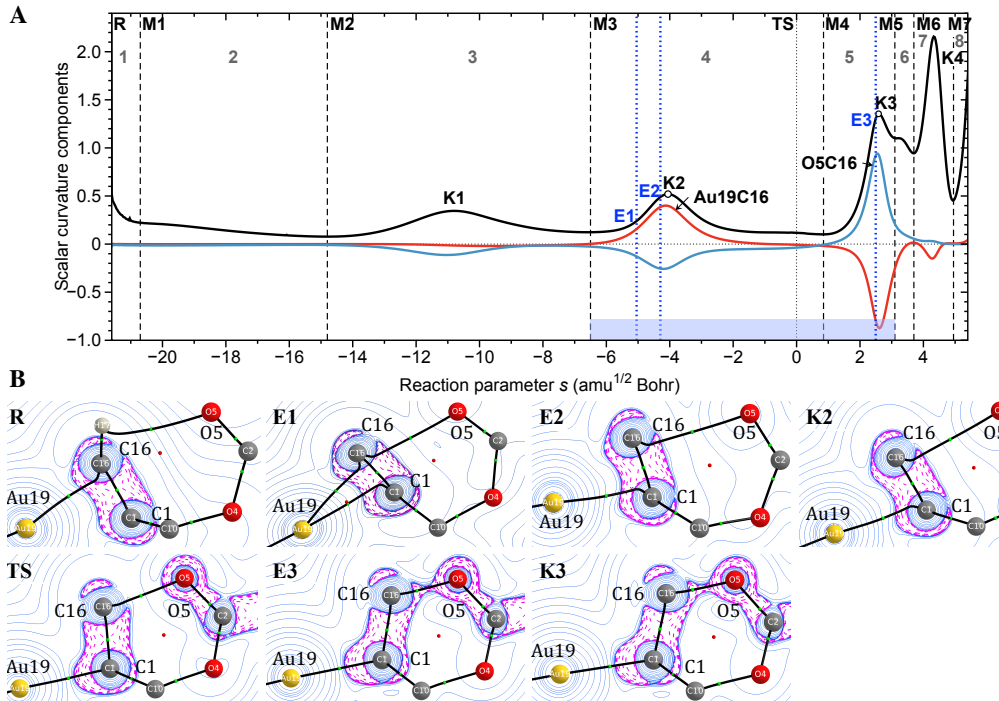


Fig. S6: R10-Step 1 A) Scalar curvature as a function of the reaction parameter s (solid black line). The decomposition of scalar curvature into components is given in color. The borders of the reaction phases are indicated by vertical dashed lines at curvature points M1, M2, M3, etc. The TS at $s = 0$ amu $^{1/2}$ Bohr is also indicated by a vertical dashed line. R marks the first curvature point, corresponding to reactant. K1, K2, etc. denote curvature peaks. E1, E2, etc. denote special points in electron density shown by blue vertical dashed lines. Values in grey 1, 2, 3, etc. indicate reaction phases and highlighted region in blue shows the chemical phases. B) Laplacian contour plots of selected curvature points R, E1, E2, K2, TS, E3, and K3, plotted in the planes C1-C16-Au19 for R-K2 and O5-C1-C16 for TS-K3. The dashed (pink) contours denote regions of charge concentration where $\nabla^2\rho(\mathbf{r}) < 0$, and the solid (blue) contours denote regions of charge depletion where $\nabla^2\rho(\mathbf{r}) > 0$.

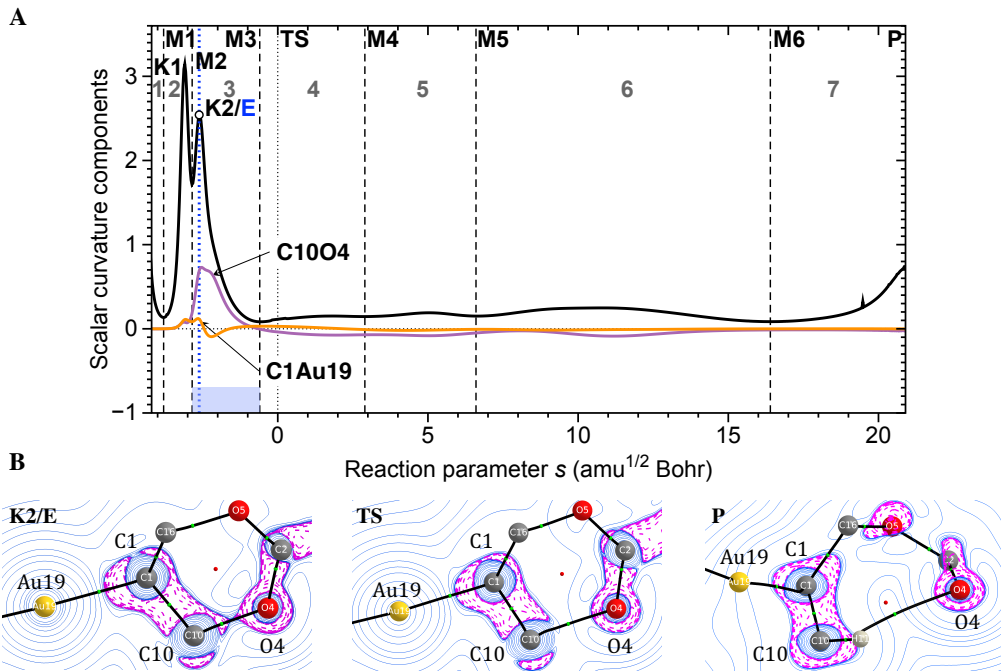


Fig. S7: R10-Step 2 A) Scalar curvature as a function of the reaction parameter s (solid black line). The decomposition of scalar curvature into components is given in color. The borders of the reaction phases are indicated by vertical dashed lines at curvature points M1, M2, M3, etc. The TS at $s = 0$ amu $^{1/2}$ Bohr is also indicated by a vertical dashed line. P marks the last curvature point, corresponding to product. K1, K2, etc. denote curvature peaks. E denotes a special point in electron density shown by a blue vertical dashed line. Values in grey 1, 2, 3, etc. indicate reaction phases and highlighted region in blue shows the chemical phases. B) Laplacian contour plots of selected curvature points K2, TS, and P, plotted in the C1-C10-O4 plane. The dashed (pink) contours denote regions of charge concentration where $\nabla^2 \rho(\mathbf{r}) < 0$, and the solid (blue) contours denote regions of charge depletion where $\nabla^2 \rho(\mathbf{r}) > 0$.

Table S7: The shift of E points denoting electron density changes relative to the corresponding curvature peaks K indicating bond formation/cleavage^a

Reaction	Bond formation		Bond cleavage		$\Delta(R, P)$
	$+\Delta s$	$\frac{\Delta s}{\Delta(R, P)} \%$	$-\Delta s$	$\frac{\Delta s}{\Delta(R, P)} \%$	
R1	0.0999	2	0.0999	2	5.3598
R2	0.7597	11	0.4998	7	6.6797
R3	0.0000	0	0.0000	0	7.5818
R4	0.7399	10	-	-	7.6462
R5	2.8794	7	1.2596	3	41.3678
R6	4.0198	23	-	-	17.3088
R7	3.2993	26	-	-	12.5071
R8(1)^b	2.8800	16	-	-	18.0768
R8(2)^b	1.0174	6	-	-	18.0768
R9	0.4499	1	0.5696	2	35.8737
R10	0.0900 ^c	0	0.0000 ^d	0	27.2101

^a Δs is used to quantify the shift of E points relative to corresponding bond formation/cleavage peaks. E points located before a corresponding bond formation curvature peak are defined by a positive value ($+\Delta s$) and vice versa. $\Delta_{R,P}$ gives the difference in path parameter s from reactant to product. Shift of the E points is expressed as a percentage of $\Delta_{R,P}$ for comparative purposes. Reaction parameter s , Δs , and $\Delta_{R,P}$ values are given in amu^{1/2}Bohr (s units).

^b **R8(1):** C2C3 bond formation; **R8(2):** O4C1 bond formation.

^c O5C16 bond formation in step 1.

^d O4C10 bond cleavage in step 2.

Coordinates of the stationary points for the reactions R1-R10¹

R1 reactant:

SCF Energy: -1038.98736
 Num. Imaginary Frequencies: 0
 H 0.00000 0.00000 1.38414
 H 0.00000 0.00000 0.65048
 H 0.00000 0.00002 -2.03462

R1 TS:

SCF Energy: -1023.79348
 Num. Imaginary Frequencies: 1
 H 0.91582 0.00000 0.00000
 H 0.00000 0.00000 0.00000
 H -0.91582 -0.00001 0.00000

R2 reactant:

SCF Energy: -25634.27697
 Num. Imaginary Frequencies: 0
 C 0.00000 0.46970 0.00000
 H 0.00000 -2.37411 0.00000
 H 1.07450 0.48381 0.00000
 H -0.53725 0.48381 0.93055
 H -0.53725 0.48381 -0.93055
 H 0.00000 -3.10862 0.00000

R2 TS:

SCF Energy: -25619.64874
 Num. Imaginary Frequencies: 1
 C 0.00000 0.26433 0.00000
 H 0.00000 -1.13402 0.00000
 H 1.05096 0.51894 0.00000
 H -0.52548 0.51894 0.91015
 H -0.52548 0.51894 -0.91015
 H 0.00000 -2.00877 0.00000

R2 product:

SCF Energy: -25641.73398
 Num. Imaginary Frequencies: 0
 C 0.00000 0.31420 0.00000
 H 0.00000 -0.77072 0.00000
 H 1.02337 0.67607 0.00000
 H -0.51168 0.67607 0.88626
 H -0.51168 0.67607 -0.88626
 H 0.00000 -3.43722 0.00000

R3 reactant:

SCF Energy: -68682.77038
 Num. Imaginary Frequencies: 0
 N -0.13504 0.48836 0.00000
 N 0.16465 -0.59545 0.00000

H -0.41143 1.48789 0.00000

R3 TS:

SCF Energy: -68630.77266
 Num. Imaginary Frequencies: 1
 N 0.07605 0.57592 0.00000
 N 0.07605 -0.57592 0.00000
 H -1.06465 0.00000 0.00000

R3 product:

SCF Energy: -68682.77038
 Num. Imaginary Frequencies: 0
 N 0.16465 0.59545 0.00000
 N -0.13504 -0.48836 0.00000
 H -0.41143 -1.48789 0.00000

R4 reactant:

SCF Energy: -58462.61205
 Num. Imaginary Frequencies: 0
 C -0.14056 0.55327 0.00000
 N 0.14944 -0.58823 0.00000
 H -0.40277 1.58537 0.00000

R4 TS:

SCF Energy: -58407.46531
 Num. Imaginary Frequencies: 1
 C 0.07986 0.62172 0.00000
 N 0.07986 -0.57498 0.00000
 H -1.03818 0.29456 0.00000

R4 product:

SCF Energy: -58442.54218
 Num. Imaginary Frequencies: 0
 C 0.18776 0.67151 0.00000
 N -0.13207 -0.47232 0.00000
 H -0.40070 -1.43307 0.00000

R5 reactant:

SCF Energy: -712265.2545
 Num. Imaginary Frequencies: 0
 C -0.15315 1.53966 1.10692
 Au 0.08239 -0.13660 -0.15138
 Cl 1.24542 -1.31870 1.45509
 C -1.38386 1.37892 1.94871
 Cl -1.05285 0.85658 -1.89801
 H 0.79396 1.51422 1.65772
 H -0.19637 2.34666 0.36691
 H -2.30111 1.32410 1.34562
 H -1.45709 2.28517 2.58330

¹ SCF energies in kcal/mol

H -1.32235 0.50901 2.61725

R5 TS:

SCF Energy: -712261.9123
 Num. Imaginary Frequencies: 1
 C 2.23774 0.23441 0.00000
 Au 0.07977 -0.15617 0.00000
 Cl -2.14749 -0.89166 0.00000
 C 2.18496 -1.17475 0.00000
 Cl -0.38098 2.16167 0.00000
 H 2.43894 0.77548 -0.92815
 H 2.43894 0.77548 0.92816
 H 2.35304 -1.72978 0.92765
 H 2.35305 -1.72977 -0.92766
 H 0.56178 -1.70259 0.00000

C 1.57427 0.69287 -0.22773
 H 2.07497 -1.23447 0.56881
 H 1.47141 -1.23537 -1.16015
 H 2.07536 1.23381 0.56882
 H 1.47180 1.23492 -1.16014
 C -0.44500 -1.43593 0.48930
 C -0.44455 1.43607 0.48931
 C -1.32252 -0.70288 -0.28916
 C -1.32230 0.70329 -0.28916
 H -0.39264 -2.51545 0.37886
 H -0.12406 -1.06597 1.45551
 H -0.39186 2.51557 0.37889
 H -0.12373 1.06599 1.45552
 H -1.87273 -1.21305 -1.07752
 H -1.87235 1.21364 -1.07751

R5 product:

SCF Energy: -712295.9848
 Num. Imaginary Frequencies: 0
 C -1.36373 1.89124 0.11249
 Au 0.00046 0.03420 0.24664
 Cl 1.34717 -1.84308 0.06650
 C -1.09182 1.70608 1.45065
 Cl -0.36764 0.20391 -2.13576
 H -0.78151 2.58469 -0.49789
 H -2.27448 1.49897 -0.34477
 H -1.78982 1.16971 2.09913
 H -0.28977 2.26061 1.94525
 H 0.29630 -0.15584 1.78086

R6 product:

SCF Energy: -147247.20398
 Num. Imaginary Frequencies: 0
 C 1.22674 -0.77758 -0.08640
 C 1.22698 0.77719 -0.08639
 H 2.02094 -1.16235 0.56292
 H 1.45326 -1.13720 -1.09561
 H 2.02130 1.16171 0.56293
 H 1.45362 1.13675 -1.09560
 C -0.12724 -1.39225 0.34812
 C -0.12680 1.39229 0.34813
 C -1.28164 -0.66819 -0.29861
 C -1.28144 0.66859 -0.29860
 H -0.14349 -2.46240 0.11761
 H -0.21862 -1.31535 1.44248
 H -0.14272 2.46245 0.11764
 H -0.21821 1.31540 1.44249
 H -2.08989 -1.23762 -0.75133
 H -2.08951 1.23828 -0.75132

R6 reactant:

SCF Energy: -147207.41404
 Num. Imaginary Frequencies: 0
 C 2.42868 -0.66595 -0.37285
 C 2.42886 0.66519 -0.37279
 H 3.19032 -1.23886 0.15005
 H 1.66373 -1.23487 -0.89239
 H 3.19065 1.23784 0.15017
 H 1.66406 1.23435 -0.89228
 C -0.96998 -1.54577 0.58315
 C -0.96962 1.54608 0.58324
 C -1.65587 -0.73507 -0.23440
 C -1.65546 0.73559 -0.23456
 H -1.04897 -2.62465 0.49634
 H -0.31056 -1.16901 1.35905
 H -1.04790 2.62499 0.49610
 H -0.31099 1.16913 1.35971
 H -2.29378 -1.19320 -0.98897
 H -2.29267 1.19391 -0.98960

R7 reactant:

SCF Energy: -170386.01560
 Num. Imaginary Frequencies: 0
 C -1.67838 -1.09353 -0.25681
 C -1.36609 -0.87988 1.02609
 C -0.03726 -0.71988 1.60974
 C 1.05184 -0.04815 1.17701
 C 1.28819 0.81385 0.01765
 C 0.68674 0.91682 -1.14667
 C 0.20194 1.07339 -2.34547
 H -2.17708 -0.87847 1.75342
 H 0.06674 -1.17573 2.59277
 H 1.90313 -0.06801 1.85231
 H 2.12260 1.50323 0.15437
 H -0.92605 -1.17726 -1.02819
 H -2.71180 -1.21625 -0.56171
 H -0.64150 1.73009 -2.53743

R6 TS:

SCF Energy: -147188.33418
 Num. Imaginary Frequencies: 1
 C 1.57406 -0.69336 -0.22774

H 0.61388 0.53680 -3.19653

R7 TS:

SCF Energy: -170374.15478
 Num. Imaginary Frequencies: 1
 C -1.27228 -0.76402 -0.40345
 C -1.26031 -0.76298 0.97376
 C -0.04796 -0.74309 1.68914
 C 1.08938 -0.13214 1.18975
 C 1.15772 0.66941 0.01905
 C 0.30913 0.71496 -1.03871
 C 0.11369 1.01417 -2.31060
 H -2.19069 -0.66064 1.52814
 H -0.04399 -1.02782 2.73698
 H 1.93842 -0.04946 1.86134
 H 1.87624 1.48897 0.06774
 H -0.51080 -1.32376 -0.92412
 H -2.19364 -0.60985 -0.95510
 H -0.86065 1.29424 -2.69548
 H 0.92099 0.93226 -3.03566

R7 product:

SCF Energy: -170421.92604
 Num. Imaginary Frequencies: 0
 C -1.09657 -0.50254 -0.55630
 C -1.14916 -0.83319 0.91257
 C -0.10563 -0.61213 1.72324
 C 1.11166 0.01757 1.22048
 C 1.18684 0.49187 -0.03994
 C 0.06639 0.39178 -0.97036
 C 0.07595 1.04191 -2.14665
 H -2.05221 -1.30447 1.28710
 H -0.15181 -0.89254 2.77001
 H 1.95335 0.13195 1.89488
 H 2.07994 1.00561 -0.38134
 H -1.01737 -1.45340 -1.10622
 H -2.04509 -0.06323 -0.88158
 H -0.76404 1.00022 -2.83140
 H 0.93185 1.63220 -2.45459

R8 reactant:

SCF Energy: -154308.47792
 Num. Imaginary Frequencies: 0
 C -0.39354 -1.84900 0.00000
 C 1.09940 1.53410 0.00000
 C 0.63750 -2.47488 0.00000
 O -1.25153 1.20176 0.00000
 N -0.05090 1.36624 0.00000
 H 1.52817 -3.05973 0.00000
 H 2.15819 1.62245 0.00000
 H -1.26403 -1.23054 0.00000

R8 TS:

SCF Energy: -154294.31838

Num. Imaginary Frequencies: 1
 C -0.54763 -1.50668 0.00000
 C 1.11674 0.78225 0.00000
 C 0.67451 -1.39704 0.00000
 O -1.18850 0.83144 0.00000
 N -0.02087 1.18320 0.00000
 H 1.68487 -1.74595 0.00000
 H 2.11002 1.19061 0.00000
 H -1.60248 -1.64979 0.00000

R8 product:

SCF Energy: -154392.08657
 Num. Imaginary Frequencies: 0
 C -0.66262 -0.92134 0.00000
 C 1.05947 0.41195 0.00000
 C 0.69650 -0.96450 0.00000
 O -1.09255 0.35321 0.00000
 N 0.01527 1.20722 0.00000
 H 1.33974 -1.83020 0.00000
 H 2.04931 0.84994 0.00000
 H -1.43225 -1.67933 0.00000

R9 reactant:

SCF Energy: -241673.80372
 Num. Imaginary Frequencies: 0
 C 1.75166 0.22319 0.51689
 C -1.43743 0.06293 0.19247
 H 2.09329 -0.58147 1.16850
 O -0.38445 -0.76503 -0.01577
 O -1.45691 1.23384 -0.12817
 C -2.56728 -0.66614 0.87869
 H -2.74560 -1.63647 0.40818
 H -2.29469 -0.85079 1.92331
 H -3.46797 -0.05321 0.84481
 C 0.83142 -0.19110 -0.59954
 H 0.53844 0.68348 -1.18514
 C 1.42501 -1.27578 -1.49149
 H 0.71213 -1.56606 -2.26911
 H 2.33519 -0.90378 -1.97179
 H 1.68138 -2.16517 -0.90656
 C 2.15671 1.47803 0.72486
 H 1.81455 2.29673 0.09676
 H 2.83706 1.72855 1.53361

R9 TS:

SCF Energy: -241636.46254
 Num. Imaginary Frequencies: 1
 C 1.28274 0.96047 0.55522
 C -1.30881 -0.22347 -0.18568
 H 1.33983 0.83129 1.63309
 O -0.32011 -0.94885 -0.54092
 O -1.35327 1.04392 -0.27942
 C -2.50585 -0.92925 0.42926
 H -2.60886 -1.93703 0.01960

H -2.34765 -1.01471 1.51146
 H -3.41758 -0.35114 0.26129
 C 1.57408 -0.11877 -0.28419
 H 1.57689 0.07132 -1.35341
 C 2.26715 -1.36147 0.15995
 H 1.89753 -2.22459 -0.39813
 H 3.34145 -1.26019 -0.04869
 H 2.13691 -1.54130 1.23003
 C 0.50394 1.96637 0.01389
 H 0.51351 2.15343 -1.05279
 H 0.07550 2.74906 0.62956

H 1.39983 -1.88846 -1.49625
 Au -0.38309 -0.30986 -0.17760
 C -4.31593 1.28958 0.02592
 C -4.57011 0.03061 0.47618
 H -4.97540 2.12953 -0.12881
 H -5.49260 -0.43326 0.78955
 C -2.36505 0.16616 0.04291
 N -2.95933 1.35572 -0.23451
 N -3.36333 -0.64491 0.47955
 C -2.29094 2.55432 -0.74969
 H -1.22446 2.35147 -0.83951
 H -2.69390 2.80965 -1.73246
 H -2.44470 3.38736 -0.06012
 C -3.21772 -2.04131 0.90045
 H -2.17090 -2.32844 0.80926
 H -3.53350 -2.14888 1.94064
 H -3.82644 -2.68513 0.26150

R9 product:

SCF Energy: -241674.44880
 Num. Imaginary Frequencies: 0
 C 1.56116 0.02605 0.15944
 C -1.64687 0.28079 0.29869
 H 1.97802 -0.28756 1.11694
 O -1.67436 0.14046 -0.90719
 O -0.60009 0.81136 0.97591
 C -2.75707 -0.11058 1.24357
 H -3.65218 -0.35361 0.67107
 H -2.44707 -0.98715 1.82239
 H -2.96328 0.69560 1.95248
 C 1.93138 -0.59308 -0.96760
 H 1.48401 -0.26932 -1.90820
 C 2.91987 -1.71892 -1.05335
 H 2.45765 -2.60966 -1.49717
 H 3.76675 -1.45062 -1.69759
 H 3.31200 -1.98989 -0.06819
 C 0.58570 1.16322 0.20050
 H 0.27796 1.46273 -0.80326
 H 0.99516 2.02475 0.73497

R10-step1 TS:

SCF Energy: -518058.01154
 Num. Imaginary Frequencies: 1
 C 1.74352 -0.38510 -0.00193
 C 4.53875 0.03673 -0.37081
 H 1.88953 -1.43565 0.26657
 O 3.95290 0.28447 0.79204
 O 3.95758 -0.00828 -1.46934
 C 6.01211 -0.21681 -0.25069
 H 6.46337 0.48008 0.45909
 H 6.16498 -1.23214 0.13295
 H 6.48173 -0.13310 -1.23082
 C 2.49279 0.55400 0.92738
 H 2.36436 1.59514 0.61176
 C 2.20666 0.39521 2.40828
 H 2.86699 1.03268 3.00132
 H 1.17009 0.68211 2.60859
 H 2.34703 -0.64298 2.72390
 C 1.97694 -0.09224 -1.36495
 H 1.93422 0.93131 -1.72136
 H 1.86704 -0.85617 -2.12864
 Au -0.41322 -0.13121 -0.08570
 C -4.56106 0.88162 -0.05542
 C -4.66172 -0.46504 0.10283
 H -5.32234 1.64391 -0.11477
 H -5.52748 -1.10025 0.20829
 C -2.46669 0.04027 -0.04038
 N -3.20994 1.17390 -0.14055
 N -3.36999 -0.96421 0.11027
 C -2.68427 2.52823 -0.31949
 H -1.59689 2.47660 -0.36051
 H -3.06214 2.95357 -1.25239
 H -2.98612 3.15876 0.52037
 C -3.05211 -2.38555 0.26184
 H -1.97088 -2.50911 0.21116
 H -3.41314 -2.74689 1.22781

R10-step1 reactant:

SCF Energy: -518071.23609
 Num. Imaginary Frequencies: 0
 C 1.88166 -0.73479 0.24770
 C 4.68520 0.50492 -0.26995
 H 1.84344 -1.60267 0.90751
 O 3.97233 0.22255 0.86553
 O 4.16028 0.92264 -1.28078
 C 6.15092 0.23716 -0.07182
 H 6.54867 0.90904 0.69548
 H 6.30624 -0.78710 0.27942
 H 6.67815 0.39836 -1.01158
 C 2.54856 0.50029 0.83816
 H 2.38109 1.36109 0.18536
 C 2.13414 0.79235 2.27282
 H 2.68662 1.65527 2.65275
 H 1.06388 1.01798 2.32434
 H 2.34237 -0.06293 2.92315
 C 1.61850 -0.90232 -1.09247
 H 1.85971 -0.11624 -1.80368

H -3.51968 -2.95785 -0.54291

R10-step1 product:

SCF Energy: -518062.98978
 Num. Imaginary Frequencies: 0
 C 1.77355 -0.32796 0.02023
 C 4.51997 0.00411 -0.33710
 H 1.96257 -1.32916 0.43157
 O 4.01356 0.53255 0.71209
 O 3.85090 -0.36101 -1.37090
 C 5.99453 -0.22110 -0.36246
 H 6.49733 0.50238 0.28053
 H 6.19661 -1.22762 0.02373
 H 6.36671 -0.16640 -1.38661
 C 2.45572 0.69473 0.87928
 H 2.32062 1.71583 0.51252
 C 2.25975 0.60673 2.37655
 H 2.92261 1.29938 2.90089
 H 1.22503 0.87227 2.60989
 H 2.44476 -0.40854 2.73936
 C 2.32193 -0.24566 -1.37005
 H 2.14959 0.70701 -1.87492
 H 2.03908 -1.07108 -2.01997
 Au -0.34752 -0.10454 -0.01450
 C -4.51401 0.84029 -0.27378
 C -4.60668 -0.45407 0.13035
 H -5.28011 1.56717 -0.49475
 H -5.46907 -1.07132 0.32876
 C -2.40868 0.04807 -0.04199
 N -3.16266 1.13059 -0.37400
 N -3.30996 -0.92277 0.26741
 C -2.64262 2.43457 -0.78438
 H -1.55413 2.38864 -0.78116
 H -2.99272 2.67616 -1.79116
 H -2.97576 3.20639 -0.08588
 C -2.98124 -2.28543 0.68739
 H -1.89695 -2.38579 0.72238
 H -3.39553 -2.47956 1.67988
 H -3.38905 -3.00481 -0.02721

R10-step2 reactant:

SCF Energy: -518062.99138
 Num. Imaginary Frequencies: 0
 C 1.77413 -0.28328 -0.16013
 C 4.52154 0.18990 -0.25412
 O 3.85824 0.47053 -1.31766
 C 5.99670 0.01685 -0.39420
 H 6.37372 0.63897 -1.20737
 H 6.49475 0.25160 0.54734
 H 6.19917 -1.03238 -0.64155
 H 2.31403 1.12857 1.39998
 C 2.24684 -0.83705 2.31631
 H 2.90665 -0.56087 3.14242
 H 1.21091 -0.74647 2.65431

H 2.43105 -1.88083 2.04565
 C 2.32917 0.56672 -1.26003
 H 2.15742 1.63851 -1.14183
 H 2.05115 0.25052 -2.26325
 C 2.44975 0.07804 1.12915
 O 4.00891 0.03663 0.90781
 H 1.96353 -1.34246 -0.38285
 Au -0.34719 -0.07758 -0.07346
 C -4.51555 0.87069 0.13854
 C -4.60523 -0.46835 -0.07641
 H -5.28328 1.61751 0.26867
 H -5.46615 -1.11199 -0.16939
 C -2.40851 0.06472 -0.01806
 C -2.64805 2.53151 0.38061
 H -2.98858 2.91628 1.34523
 H -1.55943 2.49016 0.37125
 H -2.99323 3.19150 -0.41932
 C -2.97572 -2.35107 -0.40218
 H -3.39361 -2.67976 -1.35704
 H -1.89124 -2.45206 -0.42859
 H -3.37791 -2.96760 0.40561
 N -3.16497 1.17933 0.17153
 N -3.30750 -0.94499 -0.16952

R10-step2 TS:

SCF Energy: -518060.74276
 Num. Imaginary Frequencies: 1
 C 1.73140 -0.28833 -0.20679
 C 4.54149 0.24567 -0.25177
 O 3.79049 0.57184 -1.28312
 C 5.99512 0.08742 -0.57781
 H 6.31029 0.84725 -1.29607
 H 6.58784 0.14302 0.33542
 H 6.14582 -0.89558 -1.03915
 H 2.15630 0.88708 1.55087
 C 2.19213 -1.21648 2.15976
 H 2.96994 -1.04811 2.90783
 H 1.22722 -1.20184 2.68049
 H 2.32714 -2.19997 1.70349
 C 2.32633 0.74886 -1.13334
 H 2.18134 1.77199 -0.77526
 H 1.97186 0.66907 -2.15913
 C 2.19895 -0.12074 1.14228
 O 4.11124 0.05853 0.90506
 H 1.89581 -1.30386 -0.58356
 Au -0.41372 -0.08262 -0.06486
 C -4.57094 0.87165 0.15314
 C -4.66372 -0.43217 -0.22015
 H -5.33696 1.60561 0.34967
 H -5.52609 -1.05171 -0.41147
 C -2.46895 0.06834 -0.03924
 C -2.70152 2.47547 0.64062
 H -3.06305 2.74370 1.63638
 H -1.61317 2.42886 0.65119

H -3.02522	3.22833	-0.08232	C 2.41426	0.40172	-1.16710
C -3.04050	-2.28100	-0.72305	H 2.26472	1.41238	-0.78018
H -3.42692	-2.48612	-1.72441	H 1.96393	0.30746	-2.15609
H -1.95691	-2.39387	-0.72425	C 1.75581	-0.43957	1.15065
H -3.47745	-2.98404	-0.00971	O 4.27988	1.30466	0.51768
N -3.22030	1.16151	0.25880	H 1.88516	-1.67131	-0.58231
N -3.36779	-0.90834	-0.33356	Au -0.34667	-0.19210	0.12345

R10-step2 product:

SCF Energy:	-518072.28007				
Num. Imaginary Frequencies:	0				
C 1.87369	-0.64562	-0.20999	C -4.56359	-0.14829	-0.41213
C 4.67580	0.70317	-0.45916	H -5.02872	2.02273	-0.33892
O 3.82108	0.16976	-1.38546	H -5.47681	-0.70257	-0.56422
C 6.10989	0.45043	-0.83119	C -2.35321	0.15506	-0.10795
H 6.34918	0.98776	-1.75461	C -2.34415	2.66716	0.04917
H 6.75910	0.79629	-0.02739	H -2.74458	3.16434	0.93565
H 6.27355	-0.61402	-1.02184	H -1.27152	2.52177	0.17114
H 1.95751	0.56485	1.52260	H -2.52824	3.28306	-0.83404
C 1.66856	-1.52663	2.18421	C -3.14662	-2.21996	-0.35903
H 2.64558	-1.59425	2.68135	H -3.45493	-2.58722	-1.34068
H 0.93679	-1.29288	2.96311	H -2.09249	-2.44645	-0.20358
H 1.43790	-2.50274	1.74991	H -3.73970	-2.70536	0.41932
			N -2.98296	1.35851	-0.11726
			N -3.33289	-0.76802	-0.28989

Bibliography

- [1] R. F. W. Bader, *Acc. Chem. Res.*, 1985, **18**, 9–15.
- [2] D. Cremer and E. Kraka, in *Theoretical Models of Chemical Bonding. The Concept of the Chemical Bond*, Springer Verlag, Heidelberg, 1990, vol. 2, p. 453.
- [3] R. F. Bader, T. S. Slee, D. Cremer and E. Kraka, *J. Am. Chem. Soc.*, 1983, **105**, 5061–5068.
- [4] C. Silva López, O. Nieto Faza, F. P. Cossío, D. M. York and A. R. De Lera, *Chem. Eur. J.*, 2005, **11**, 1734–1738.
- [5] M. F. Zalazar and N. M. Peruchena, *J. Mol. Model.*, 2011, **17**, 2501–2511.
- [6] R. H. Crabtree, *The Organometallic Chemistry of the Transition Metals*, John Wiley & Sons, New Jersey, 2005, pp. 1–546.
- [7] E. Sosa Carrizo, F. Bickelhaupt and I. Fernández, *Chem. Eur. J.*, 2015, **21**, 14237–14237.
- [8] R. Kumar, J. P. Krieger, E. Gómez-Bengoa, T. Fox, A. Linden and C. Nevado, *Angew. Chem. Int. Edit.*, 2017, **56**, 12862–12865.
- [9] F. Rekhroukh, L. Estevez, S. Mallet-Ladeira, K. Miqueu, A. Amgoune and D. Bourissou, *J. Am. Chem. Soc.*, 2016, **138**, 11920–11929.
- [10] M. Castiñeira Reis, C. S. López, E. Kraka, D. Cremer and O. N. Faza, *Inorga. Chem.*, 2016, **55**, 8636–8645.
- [11] R. F. Bader, *Atoms in Molecules: A Quantum Theory*, Clarendon Press, Oxford, U.K., 1990.
- [12] M. Mousavi and G. Frenking, *Organometallics*, 2013, **32**, 1743–1751.
- [13] L. J. Farrugia, C. Evans and M. Tegel, *J. Phys. Chem. A*, 2006, **110**, 7952–7961.
- [14] R. B. Woodward and R. Hoffmann, *Angew. Chem. Int. Edit.*, 1969, **8**, 781–932.
- [15] K. Fukui, *Angew. Chem. Int. Edit.*, 1982, **21**, 801–809.
- [16] S. Berski, J. Andrés, B. Silvi and L. R. Domingo, *J. Phys. Chem. A*, 2003, **107**, 6014–6024.
- [17] F. De Proft, P. W. Ayers, S. Fias and P. Geerlings, *J. Chem. Phys.*, 2006, **125**, 214101.
- [18] E. Kraka, A. Wu and D. Cremer, *J. Phys. Chem. A*, 2003, **107**, 9008–9021.
- [19] T. Sexton, E. Kraka and D. Cremer, *J. Phys. Chem. A*, 2016, **120**, 1097–1111.
- [20] J. A. Ross, R. P. Seiders and D. M. Lemal, *J. Am. Chem. Soc.*, 1976, **98**, 4325–4327.
- [21] S. Sakai, *Theor. Chem. Acc.*, 2008, **120**, 177–183.
- [22] J. A. Duncan, D. E. G. Calkins and M. Chavarha, *J. Am. Chem. Soc.*, 2008, **130**, 6740–6748.
- [23] C. S. López, O. N. Faza, M. Freindorf, E. Kraka and D. Cremer, *J. Org. Chem.*, 2016, **81**, 404–414.
- [24] D. H. Ess and K. N. Houk, *J. Phys. Chem. A*, 2005, **109**, 9542–9553.
- [25] D. H. Ess and K. N. Houk, *J. Am. Chem. Soc.*, 2008, **130**, 10187–10198.
- [26] A. de Cózar and F. P. Cossío, *Phys. Chem. Chem. Phys.*, 2011, **13**, 10858–10868.
- [27] Y. Lan, L. Zou, Y. Cao and K. N. Houk, *J. Phys. Chem. A*, 2011, **115**, 13906–13920.
- [28] M. Freindorf, T. Sexton, E. Kraka and D. Cremer, *Theor. Chem. Acc.*, 2013, **133**, 1423–1441.
- [29] T. M. Sexton, M. Freindorf, E. Kraka and D. Cremer, *J. Phys. Chem. A*, 2016, **120**, 8400–8418.
- [30] M. Freindorf, D. Cremer and E. Kraka, *Mol. Phys.*, 2017, **116**, 611–630.